Available online at www.sciencedirect.com
ScienceDirect
Journal of Power Sources 163 (2007) 907–915
JOURNAL OF POWER SOURCES
www.elsevier.com/locate/jpowsour

# A three-dimensional two-phase flow model for a liquid-fed direct methanol fuel cell

Jiabin Ge, Hongtan Liu *

*Department of Mechanical and Aerospace Engineering, University of Miami, Coral Gables, USA*

Received 10 August 2006; received in revised form 3 October 2006; accepted 4 October 2006
Available online 13 November 2006

**Abstract**

A three-dimensional, two-phase, multi-component model has been developed for a liquid-fed DMFC. The modeling domain consists of the membrane, two catalyst layers, two diffusion layers, and two channels. Both liquid and gas phases are considered in the entire anode, including the channel, the diffusion layer and the catalyst layer; while at the cathode, two phases are considered in the gas diffusion layer and the catalyst layer but only single gas phase is considered in the channels. For electrochemical kinetics, the Tafel equation incorporating the effects of two phases is used at both the cathode and anode sides. At the anode side the presence of gas phase reduces the active catalyst areas, while at the cathode side the presence of liquid water reduces the active catalyst areas. The mixed potential effects due to methanol crossover are also included in the model. The results from the two-phase flow mode fit the experimental results better than those from the single-phase model. The modeling results show that the single-phase models over-predict methanol crossover. The modeling results also show that the porosity of the anode diffusion layer plays an important role in the DMFC performance. With low diffusion layer porosity, the produced carbon dioxide cannot be removed effectively from the catalyst layer, thus reducing the active catalyst area as well as blocking methanol from reaching the reaction zone. A similar effect exits in the cathode for the liquid water.


*Keywords:* DMFC; Fuel cell; Fuel cell model

## 1. Introduction

Efforts in developing mathematical models for DMFC have been limited until recent years. Baxter et al. [1] developed a one-dimensional, single-phase mathematical model for a liquid-fed DMFC, focused on the anode catalyst layer. Dohle et al. [2] presented a one-dimensional model for the vapor-fed DMFC including methanol crossover and the effects of methanol concentration on the cell performance were studied. Scott et al. [3,4] developed several simplified single-phase models to study transport and electrochemical processes in the liquid-fed DMFC and showed that the cell performance was limited by the slow diffusion of liquid methanol. Sundmacher and Scott [5] developed a model of the methanol mass transport process and the model was used to predict the effective methanol concentration at the catalyst surface and the anode polarization. This model, together with an empirical model of the open circuit voltage and the cathode overpotential model, was used to predict the overall cell voltage and current density response of the fuel cell. Cruickshank and Scott [6] presented a simple model to describe the permeation of methanol from anode to cathode in DMFC. Shukla et al. [7] developed a one-dimensional model for a comparison of the performance of a solid–polymer electrolyte DMFC with aqueous methanol and methanol mixed with air at the anode. Kulikovsky [8] simulated a vapor-fed DMFC with a two-dimensional model and compared the detailed current density distributions in the backing, catalyst layer, and membrane separator between a conventional and a new current collector. Wang and Wang [9] developed a two-dimensional, two-phase and multi-component model for a liquid-feed DMFC. In the model, the catalyst layer was considered as an infinitely thin interface. Birgersson et al. [10] developed a two-dimensional single-phase DMFC anode model, where the catalyst layer was considered as boundary conditions via parameter adaptation. Divisek et al. [11] accounted for the influence of both the methanol and oxygen reaction kinetics and their dependency

* Corresponding author. Tel.: +1 3052842019; fax: +1 3052842580.
*E-mail address:* hliu@miami.edu (H. Liu).

0378-7753/$ – see front matter © 2006 Elsevier B.V. All rights reserved.
doi:10.1016/j.jpowsour.2006.10.014

**Nomenclature**

| | |
|---|---|
| $C$ | mass fraction |
| $D$ | diffusivity ($m^2\ s^{-1}$) |
| $F$ | Faraday constant (96485.309 C $mol^{-1}$) |
| $k$ | permeability of gas diffuser ($m^2$) |
| $M$ | molar mass (kg $mol^{-1}$) |
| $P$ | pressure (Pa) |
| $P_w^{sat}$ | the saturation pressure of water at operating temperature |
| $r$ | the porous media correction factor |
| $r_c$ | advection correction factor |
| $R$ | gas constant (8.314 J $(mol\ K)^{-1}$) |
| $R_{mr}$ | resistance of membrane ($\Omega$ m) |
| $s$ | saturation |
| $S$ | source term |
| $V$ | the intrinsic velocity vector (m $s^{-1}$) |
| $X$ | mole fraction |
| $z$ | charge of the fixed sites |

*Greek letters*

| | |
|---|---|
| $\varepsilon$ | porosity |
| $\phi$ | membrane phase potential |
| $\lambda$ | the electro-osmotic drag coefficient |
| $\mu$ | viscosity (kg $(m\ s)^{-1}$) |
| $\nu$ | kinetics viscosity ($m^2\ s^{-1}$) |
| $\theta_c$ | contact angle |
| $\rho$ | density (kg $m^{-3}$) |
| $\sigma$ | surface tension (N $m^{-1}$) |
| $\xi$ | relative mobility |

*Subscripts and superscripts*

| | |
|---|---|
| a | anode, air |
| c | cathode |
| d | diffusion |
| e | effective |
| g | gas |
| $H^+$ | proton |
| $i$ | $i$th layer |
| $k$ | $k$th component |
| l | liquid water |
| m | methanol |
| mr | membrane |
| N | nitrogen |
| O | oxygen |
| w | water |

on the two-phase mass flow in the catalyst and diffusion layers by a vapor–liquid model for the DMFC. Detailed information on fuel cell modeling and transport phenomena can be found in several recent reviews [12–14].

It is well-known that reaction rate in a catalyst layer is not uniform. Therefore, to accurately modeling a fuel cell, including a DMFC, catalyst layers must be treated as parts of the modeling domain instead of boundaries or interfaces. Furthermore, a DMFC is a complex multiphase and multi-component system.

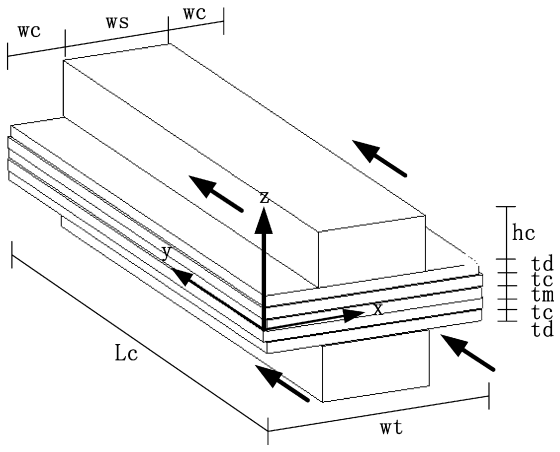


Fig. 1. The schematic of the modeling domain.

Multiphase flows are driven by buoyancy, gravitational, capillary and viscous forces. For multiphase flows in porous media, the capillary forces play fundamental roles in controlling phase distributions. A model for a DMFC without including the two-phase flow is not complete.

In this work, a three-dimensional two-phase model is developed and the modeling domain includes the two fluid channels, two diffusion layers and two catalyst layers. The model is used to study various transport phenomena in a DMFC, the cell performance and the effects of methanol crossover.

## 2. Mathematical model development

Fig. 1 shows the modeling domain for a DMFC, which consists of the anode side, cathode side and polymer electrolyte membrane. The anode side and cathode side have the same structure, which is divided into the gas channel, diffusion layer and catalyst layer. The fuel and oxidant flow along the channels, where the flows are assumed to be laminar and the gas mixtures are assumed to be perfect gases. All phases are assumed to be continuous so that the continuum approach can be applied. In the cathode side, two phases are considered in the gas diffusion layer and the catalyst layer, but in the gas channels, only gas mixture of water vapor, oxygen and nitrogen is considered and the liquid water is neglected. In the anode side, two phases, the liquid phase of mixture of water and methanol, and gas phase of carbon dioxide are considered in all the areas, including the channels, the diffusion layer and the catalyst layer.

Such parameters as gas volume fraction and liquid saturation are assumed to be volume-averaged properties to accommodate a macroscopic continuum approach in the porous media. Liquid water is assumed to be homogeneously distributed within each control volume. The liquid phase velocity is different from the gas phase velocity and the mixture velocity is the weighted average of these two.

In Fig. 1, hc is the gas channel height; td, tc, tm are the thickness of the diffusion layer, catalyst layer, and the membrane, respectively; wc is the half-width of the gas channel; ws is the width of the collector plate; and Lc is the length of the fuel cell. The reactants of anode side and cathode side enter the gas

Table 1
Geometric parameters used in the model

| | |
|---|---|
| Channel length, Lc (m) | $6.5 \times 10^{-2}$ |
| Half-channel width, wc (m) | $5.0 \times 10^{-4}$ |
| Channel height, hc (m) | $8 \times 10^{-4}$ |
| Channel shoulder width, ws (m) | $1.0 \times 10^{-3}$ |
| Diffusion layer thickness, td (m) | $1.4 \times 10^{-4}$ |
| Catalyst layer thickness, tc (m) | $3 \times 10^{-5}$ |
| Membrane thickness (Nafion®117), tm (m) | $1.8 \times 10^{-4}$ |

channels from the surface at $y = 0$. The geometric parameters are given in Table 1.

## 3. Governing equations

The governing equations include mass conservation equation, momentum equations, species conservation equations, and electrochemical kinetics equations (Tafel equation). All the conservation equations are developed for the entire solution domain of the model with source terms modified in each region to reflect the appropriate physical phenomena. These equations are similar to those used in PEM fuel cells [15,16],

$$\frac{\partial(\varepsilon\rho)}{\partial t} + \nabla \cdot (\varepsilon\rho\vec{V}) = 0 \tag{1}$$

$$\frac{\partial(\varepsilon\rho\vec{V})}{\partial t} + \nabla \cdot (\varepsilon\rho\vec{V}\vec{V}) = -\varepsilon\nabla P + \nabla \cdot (\varepsilon\mu\nabla\varepsilon\rho\vec{V}) + \rho S_i \tag{2}$$

$$\nabla \cdot (\gamma_c\rho\vec{V}C) = \nabla \cdot (\rho_l s_l D_l^e \nabla C_l) + \nabla \cdot [\rho_g s_g D_g^e \nabla C_g] - \nabla \cdot [(C_l - C_g)J_l] + S_k \tag{3}$$

where $\rho$ is the total mixture density of liquid and gas phase, $\vec{V}$ the intrinsic velocity vector, $\varepsilon$ the porosities, $P$ the pressure, $S_k$ the source terms, $\mu$ viscosity, $s_l$ liquid saturation and $s_g$ is the saturation of gaseous phase (void fraction). Note that saturation is defined as the volume fraction of a phase in the mixture and $s_l + s_g = 1$.

Eq. (1) is the mass conservation equation for the entire cell. Eq. (2) is the momentum equation in vector form, where the source term accounts for the forces exerted on the fluid by the solid matrix of a porous media and is zero in the channel. Eq. (3) is the species conservation equation, where the source term accounts for the species created/consumed by electrochemical reaction in catalyst layers and is non-zero in catalyst layers only. In the cathode diffusion layer and catalyst layer, species equations are given for oxygen, nitrogen, water vapor and liquid water; while in the anode side, species equations are given for liquid water, liquid methanol, dissolved carbon dioxide and carbon dioxide gas.

The density of the mixture of liquid and gas phase is given by,

$$\rho = \rho_l s_l + \rho_g s_g \tag{4}$$

The water saturation is given by,

$$s_w = \frac{\rho_g(C^w - C^w_{g,eq})}{\rho_l(C^w_{l,eq} - C^w) + \rho_g(C^w - C^w_{g,eq})} \tag{5}$$

and when

$$C^w < C^w_{g,eq}, \qquad s_w = 0$$

where $C^w_{g,eq}$ is the equilibrium water concentration and it is given by,

$$C^w_{g,eq} = \frac{M^w P_v(T)}{\rho_g RT} \tag{6}$$

where $P_v(T)$ is the water vapor saturation pressure at the given local temperature.

In Eq. (3) $D^e_k$ ($k$ = l or g) is the effective diffusivity of component $k$ in the porous media and it is related to its binary diffusivity by the following equation:

$$D^e_k = D_k \varepsilon^{1.5} \tag{7}$$

The advection correction factor is given by,

$$\gamma_c = \frac{\rho(\xi_l C_l + \xi_g C_g)}{\rho_l s_l C_l + \rho_g s_g C_g} \tag{8}$$

and the relative mobility are given by,

$$\xi_l(s_l) = \frac{k_{rl}/\nu_l}{(k_{rl}/\nu_l) + (k_{rg}/\nu_g)} \tag{9}$$

$$\xi_g(s_l) = 1 - \xi_l(s_l) \tag{10}$$

The relative permeabilities for liquid and gas phase are,

$$k_{rl} = s_l^3 \tag{11}$$

$$k_{rg} = s_g^3 \tag{12}$$

The fluid viscosity is given by,

$$\mu = \frac{\rho}{(k_{rl}/\nu_l) + (k_{rg}/\nu_g)} \tag{13}$$

$J_l$ in Eq. (3) is given by,

$$J_l = \frac{\xi_l \xi_g k}{\nu}[\nabla P_c + (\rho_l - \rho_g)\vec{g}] \tag{14}$$

where the capillary pressure saturation function, $P_c$, depends on the interfacial tension between the liquid water and the solid phase of the porous media. It can be determined by the pore geometry [15,17],

$$P_c(s) = P_g - P_l = \sigma\cos\theta_c\left(\frac{\varepsilon}{K}\right)^{1/2}\psi(s) \tag{15}$$

where $\sigma$ is the surface tension at the gas liquid interface, the contact angle $\theta_c$ of a liquid droplet defined as $\cos\theta_c = \sigma_{sg} - \sigma_{sl}/\sigma$, $P_g$ the pressure of gas phase, $P_l$ the pressure of the liquid phase, and $\psi(s)$ is the capillary pressure function.

The cubic Leverett function is usually used for the capillary pressure function,

$$\psi(s) = 1.417 s_g - 2.120 s_g^2 + 1.263 s_g^3 \tag{16}$$

Table 2
The source terms in the momentum equation

| Channel | $r_\varepsilon$, 1.0 | $S_i$, 0 |
|---|---|---|
| Diffuser | $2.25\left(\frac{1}{\varepsilon_d}-1\right)^2$ | $-\varepsilon_d\frac{\mu}{k}\vec{V}$ |
| Catalyst | $2.25\left(\frac{1}{\varepsilon_c}-1\right)^2$ | $-\varepsilon_c\frac{\mu}{k}\vec{V}+\frac{k_\phi}{k_h}C_{H^+}zF\nabla\phi$ |

### 3.1. Reduction of the governing equations

For steady state, the mass conservation and momentum equations are reduced to,

$$\nabla\cdot(\varepsilon\rho\vec{V})=0 \tag{17}$$

$$\rho\vec{V}\cdot\nabla\vec{V}=-\nabla P+r_s\nabla\cdot(\mu\nabla\vec{V})+\rho S_i \tag{18}$$

where the source terms are given in Table 2.

In the momentum equation and Table 2, $\varepsilon_d$ and $\varepsilon_c$ are the porosities of the diffusion layer and catalyst layer, respectively, $r_\varepsilon$ is the porous media correction factor, $k$ is the permeability of water ($k_w$) in the anode and the permeability of air ($k_{air}$) in the cathode, $k_\phi$ is electro-kinetic permeability in the membrane, $k_h$ is the hydraulic permeability in the membrane, $z$ is the charge number of the fixed sites, $C_{H^+}$ is the concentration of protons that is taken to be the concentration of the fixed charge sites, and $\phi$ is the membrane phase potential.

The individual phase velocities are calculated from,

$$\varepsilon\rho_l\vec{V}_l=J_l+\xi_l\varepsilon\rho\vec{V} \tag{19}$$

$$\varepsilon\rho_g\vec{V}_g=-J_l+\xi_g\varepsilon\rho\vec{V} \tag{20}$$

### 3.2. The species equation in the cathode side

Two gas species, oxygen and nitrogen, and the mixture of vapor and liquid water, are considered in the cathode.

Assuming only gas phase (oxygen, nitrogen and vapor) exists in the cathode gas channel, the species equation is in the same form to that for single-phase flow (Table 3),

$$\nabla\cdot(\rho_g\vec{V}_gC_g^O)=\nabla\cdot(\rho_gD_g^O\nabla C_g^O) \tag{21}$$

$$\nabla\cdot(\rho_g\vec{V}_gC_g^w)=\nabla\cdot(\rho_gD_g^w\nabla C_g^w) \tag{22}$$

$$C_g^O+C_g^w+C_g^N=1 \tag{23}$$

In the cathode gas diffusion layer and catalyst layer, two-phase flow is considered and the species are oxygen ($C^O$), nitrogen ($C^N$) and water ($C^w$).

When the dissolved oxygen in water is neglected, its concentration in the liquid phase is zero, then,

$$C_l^O=0,\qquad \rho C^O=\rho_gC_g^Os_g\quad\text{and}\quad r_c=\frac{\rho\xi_g}{\rho_gs_g}$$

From Eq. (3), the oxygen species equation becomes,

$$\nabla\cdot(\rho_g\vec{V}_gC_g^O)=\nabla\cdot[\rho_gs_gD_O^e\nabla C_g^O]+S_O \tag{24}$$

In the porous cathode electrode, the transport of liquid water is driven by two mechanisms, capillary force (driven by saturation gradient) and interfacial shear force (exerted by gas flow) [18–20]. The net water flux through the interface between the cathode catalyst layer and the GDL include the water generation rate in the catalyst layer and the net water transfer rate due to electro-osmosis and diffusion,

$$j^w=-\frac{M_w(1+a)}{2F}j_c \tag{25}$$

where $a$ is the net water transport coefficient across the membrane. Water exists in both vapor and liquid phases. For the liquid phase, the only species is water, so,

$$C_l^w=1,\qquad \nabla C_l^w=0,\quad\text{and}\quad \rho C^w=\rho_ls_w+\rho_gs_gC_g^w$$

The species equation for water becomes,

$$\nabla\cdot(\rho_g\vec{V}_gC_g^w)=\nabla\cdot[\rho_gs_gD_g^w\nabla C_g^w]-\nabla\cdot(\rho_l\vec{V}_l)+S_w \tag{26}$$

$$C^O+C^N+C^w=1 \tag{27}$$

The source terms in the species equations are given in Table 3.

### 3.3. The species equations in the anode side

Carbon dioxide gas management is an important issue in liquid-fed direct methanol fuel cell [21]. The relatively large amount of carbon dioxide reduces the free area for methanol to reach the catalyst layer. Carbon dioxide is mostly transported out to the anode channel through the catalyst layer and the diffusion layer.

For the liquid phase, the species include water, methanol and the dissolved carbon dioxide; while for the gas phase, only carbon dioxide is considered.

Thus, $C_g^c=1$

Table 3
Anode and cathode source term ($s_k$) in the species equations

| | Anode (source term $s_k$) | | | | Cathode (source term $s_k$) | |
|---|---|---|---|---|---|---|
| | Methanol | Water | Proton | Carbon dioxide | Oxygen | Water |
| Channel layers | 0 | 0 | 0 | 0 | 0 | 0 |
| Diffusion layers | 0 | 0 | 0 | 0 | 0 | 0 |
| Catalyst layers | $-\frac{M_m}{6F}j_a$ | $-\frac{M_w}{6F}j_a$ | $\frac{1}{F}j_a$ | $\frac{M_c}{6F}j_a$ | $-\frac{M_O}{4F}j_c$ | $\frac{M_w(1+\alpha)}{2F}j_c$ |

The liquid saturation is given by,

$$s_l = \frac{\rho_g(1 - C^c)}{\rho_l(C^c - C^c_{l,sat}) + \rho_g(1 - C^c)} \quad (28)$$

$s_l = 1$ if $C^c < C^c_{l,sat}$

For methanol, $C^m_g = 0$, and the species equation for liquid methanol is,

$$\nabla \cdot (\rho_l \vec{V}_l C^m_l) = \nabla \cdot (\rho_l s_l D^e_m \nabla C^m_l) + S_m \quad (29)$$

The mass fraction of carbon dioxide in the gas phase is $C^c_g = 1$.

The species equation for carbon dioxide is,

$$\nabla \cdot (\rho_l \vec{V}_l C^c_l) = \nabla \cdot (\rho_l s_l D^e_c \nabla C^c_l) - \nabla \cdot (\rho_g \vec{V}_g) + S_c \quad (30)$$

The total mass fraction of carbon dioxide is,

$$\rho C^c = \rho_l s_l C^c_l + \rho_g(1 - s_l) \quad (31)$$

And in the anode, we have

$$C^c + C^w + C^m = 1 \quad (32)$$

### 3.4. Electrochemical equations in catalyst layers

Tafel equation is used to describe reaction in both the cathode and anode catalyst layers. In the anode catalyst layer, the carbon dioxide gas block methanol from reaching the catalyst surface and thus reduce the catalyst active surface area. In the cathode catalyst layer, the presence of liquid water contributes to electrode flooding by blocking active sites on the catalysts and reducing the gas volume in the porous electrode [22]. This leads to smaller active area available for reaction and reduced area and volume for oxygen gas transport [9,18]. To account for these coverage phenomena, the term $s_l$ is included in the Tafel equation for the anode side and the term $(1 - s_w)$ is included in the Tafel equation for the cathode side. Thus,

$$j_a = a i^{ref}_a \frac{s_l C^{\gamma_a}_c}{C^{ref}_c} \exp\left(\frac{\alpha_a F}{R_c T}\eta_a\right) \quad (33)$$

$$j_c + j_p = j^O_{0,ref} \frac{(1 - s_w)\rho_g C^O_g}{\rho_{g,ref} C^O_{g,ef}} \exp\left(\frac{\alpha_c F}{RT}\eta_c\right) \quad (34)$$

where $j_p$ is the pseudo-current accounting for methanol crossover flux.

### 3.5. Cell potential and current density

The cell voltage is calculated by,

$$E_{cell} = E_0 - \eta_a - \eta_c - I R_{mr} \quad (35)$$

where $E_0$ is the difference between the half cell potentials of the anode and cathode, $R_{mr}$ the membrane resistance, and $I$ is the average current density of the cell and is given by,

$$I = \int_0^{tc} j \, dz \quad (36)$$

where tc is the catalyst layer thickness.

The ionic conductivity of Nafion® is given by [23],

$$\sigma_{mr}(T) = \sigma^{ref}_{mr} \exp\left[1268\left(\frac{1}{303} - \frac{1}{T}\right)\right] \quad (37)$$

where $\sigma^{ref}_{mr}$ is the reference ionic conductivity at 303 K and is given by,

$$\sigma^{ref}_{mr} = 0.00513\beta - 0.00326 \quad (38)$$

where the water content in the membrane, $\beta$, depends on the water activity, $\alpha$, according to the following relationship [24]:

$$\beta = 0.043 + 17.18\alpha - 39.85\alpha^2 + 36.0\alpha^3, \quad (0 < \alpha \le 1)$$

$$\beta = 14.0 + 1.4(\alpha - 1), \quad (1 < \alpha \le 3)$$

The water activity is calculated by,

$$\alpha = \frac{X^w P}{P_v(T)} \quad (39)$$

where $X^w$ is the water mole fraction.

The molecular weight of the mixture is given by,

$$M = \frac{1}{\sum C^k / M^k} \quad (40)$$

The water mole fraction is given by,

$$X^w = \frac{C^w M}{M^w} \quad (41)$$

The resistance of membrane is defined by,

$$R_{mr} = \int_0^{tm} \frac{1}{\sigma_{mr}} dz \quad (42)$$

where tm is the membrane thickness.

### 3.6. Methanol crossover

In the membrane, the methanol transports due to diffusion and electro-osmotic drag and the flux is given by [7],

$$N^{mr}_m = \frac{\lambda_m I}{F} - \varepsilon^{1.5}_{mr} D^{mr}_m \frac{dC^{mr}_m}{dz} \quad (43)$$

where $C^{mr}_m$ is the methanol concentration in the membrane.

The electro-osmotic drag coefficient ($\lambda_m$) of methanol is defined as the number of methanol molecules dragged by each proton through membrane ($CH_3OH/H^+$), and it is given by [25],

$$\lambda_m = X_m|_{z=0} \lambda_w \quad (44)$$

where $\lambda_w$ is the electro-osmotic drag coefficient for water.

The diffusion coefficient of methanol in membrane ($D^{mr}_m$) is given by [7],

$$D^{mr}_m = 4.012 \times 10^{-13} \exp(0.024312T) \, [m^2 \, s^{-1}] \quad (45)$$

### 3.7. Boundary conditions

At the anode and cathode inlets,

$$V^a = V^w_{feed}, \quad C^m_l = C^m_{feed}, \quad C^w_l = C^w_{feed} \text{ (anode)}$$

$$V^a = V^{air}_{feed}, \quad C^O_g = C^O_{feed}, \quad C^w_g = C^w_{feed} \text{ (cathode)}$$

Table 4
The parameters and properties used in the model

| Property | Value |
|---|---|
| Cell temperature, $T$ (K) | 343 |
| Pressure, $P$ (N m$^{-2}$) | $1.013 \times 10^5$ |
| Anode reactant flow rate, $Q_a^{inlet}$ (ml min$^{-1}$) | 15 |
| Cathode reactant flow rate, $Q_c^{inlet}$ (ml min$^{-1}$) | 1000 |
| Inlet oxygen mole fraction, $X_O^{inlet}$ (mol mol$^{-1}$) | 0.21 |
| Inlet methanol concentration, $C_{CH}^{inlet}$ (mol m$^{-3}$) | 1000 |
| Methanol reference concentration, $C_{CH}^{ref}$ (mol m$^{-3}$) | 2000 |
| Oxygen reference concentration, $C_O^{ref}$ (mol m$^{-3}$) | 0.472 |
| Diffusion coefficient of oxygen in air, $D_O$ (m$^2$ s$^{-1}$) | $1.22 \times 10^{-10}$ |
| Diffusion coefficient of water in air (m$^2$) | $3.32 \times 10^{-5}$ |
| Diffusion coefficient of methanol in water, $D_m$ (m$^2$ s$^{-1}$) | $2.8 \times 10^{-9}$ |
| Porosity of diffusion layer, $\varepsilon_d$ | 0.5 |
| Porosity of catalyst layer, $\varepsilon_c$ | 0.6 |
| Porosity of membrane, $\varepsilon_m$ | 0.28 |
| Permeability to air in the gas diffuser, $k_{air}$ (m$^2$) | $1.76 \times 10^{-11}$ |
| Permeability to water in the gas diffuser, $k_w$ (m$^2$) | $1.0 \times 10^{-11}$ |
| Air viscosity, $\mu_g$ (kg (m s)$^{-1}$) | $2.05 \times 10^{-5}$ |
| Electrokinetic permeability of the membrane, $k_\phi$ (m$^2$) | $7.18 \times 10^{-20}$ |
| Hydraulic permeability of the membrane, $k_h$ (m$^2$) | $1.8 \times 10^{-18}$ |
| Reference exchange current density times specific area at anode, $ai_a^{ref}$ (A m$^{-3}$) | $1.0 \times 10^6$ |
| Reference exchange current density times specific area at cathode, $ai_c^{ref}$ (A m$^{-3}$) | 200 |
| Anode reaction order, $\gamma_a$ | 1.0 |
| Cathode reaction order, $\gamma_c$ | 1.0 |
| Electro-osmotic drag coefficient of water, $\lambda_w$ | 2.5 |
| Anode transfer coefficient, $\alpha_a$ | 0.5 |
| Cathode transfer coefficient, $\alpha_c$ | 1.0 |
| Charge of fixed (sulfonate) sites, $z$ | −1 |
| Air density, $\rho_{air}$ (kg m$^{-3}$) | 1.025 |
| Water density, $\rho_{water}$ (kg m$^{-3}$) | 977.8 |
| Net water transport coefficient, $a$ | 0.5 |

At the walls and the interface with the collector plate shoulder, no-slip velocity boundary conditions are used. Neumann-type boundary conditions are used for velocity at the channel outlets. At the interface between the catalyst layer and membrane, the velocity is assumed to be zero. For all species equations, the Neumann boundary conditions are is applied at all the outlets, solid walls and symmetry surfaces.

## 4. Modeling results and discussions

### *4.1. Comparing with experimental data and single-phase model*

All parameters and properties in the model are given in Table 4. To validate the numerical model developed in the preceding section, typical modeling results are compared with our experimental data [26] for a single cell operated at 1 M methanol concentration as shown in Fig. 2. The cell temperature is 70 °C, cathode humidification temperature 70 °C, methanol flow rate 6 ml min$^{-1}$, and air flow rate 1200 SCCM. It is seen from Fig. 2 that the result from the two-phase model shows better agreement with the experimental data than the single-phase model, particularly at high current density region. Fig. 3 shows the modeling results of anode overpotential versus current density from the two phase model and the single-phase model at the same operating parameters as those in Fig. 2. In the single-phase model, only the mixture of water and methanol is considered. Carbon dioxide is created by electrochemical reaction, partly dissolved in the liquid phase. When the dissolved carbon dioxide concentration exceeds its solubility, carbon dioxide gas is emerges and partially covers the reaction sites. From Fig. 3, it can be seen that at lower anode overpotential, the corresponding current density

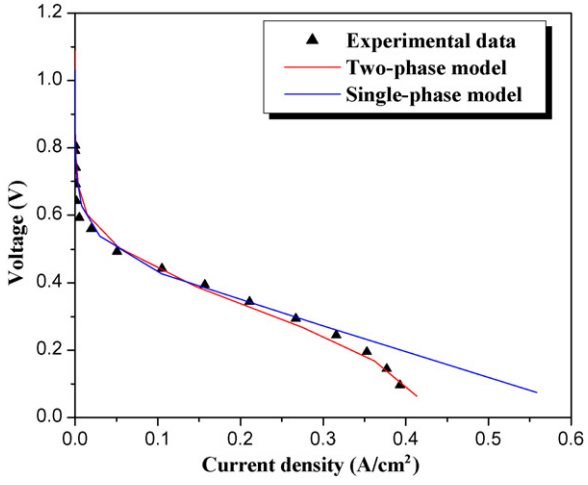


Fig. 2. Comparison of modeling results with experimental data and the results from single-phase model. Methanol feed concentration 1 M, cell temperature 70 °C, cathode humidification temperature 70 °C, methanol flow rate 6 ml min$^{-1}$, and air flow rate 1200 SCCM.

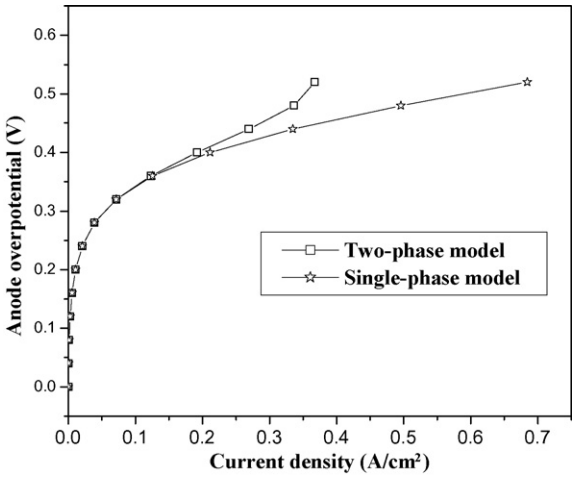


Fig. 3. Comparison of predicted of anode overpotential between the two-phase model and single-phase model. Methanol concentration 1 M, cell temperature 70 °C, methanol flow rate 6 ml min$^{-1}$, and air flow rate 1200 SCCM.

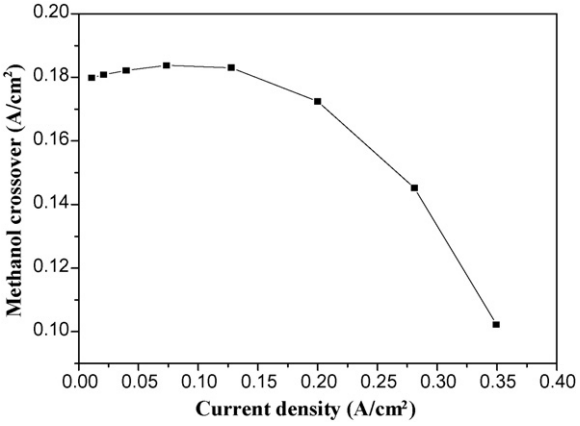


Fig. 4. Predicted methanol crossover pseudo-current density as function of cell current density. Methanol concentration 1 M, cell temperature 70 °C, methanol flow rate 6 ml min$^{-1}$, and air flow rate 1200 SCCM.

is low and the deviation of single-phase model result from that of the two phase model is negligible; while at high current density the single-phase model under-predicts the anode overpotential and the amount of under prediction increases with current density.

### 4.2. Methanol crossover

Fig. 4 shows a modeling result for methanol crossover. The flux of methanol crossover is represented with a pseudo-current density. The methanol crossover is mainly caused by

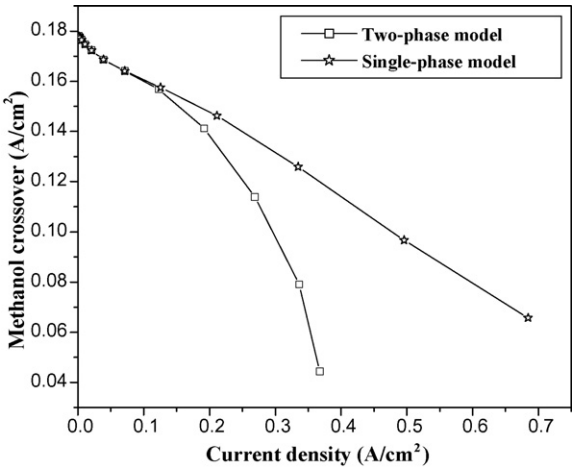


Fig. 5. The comparison of methanol crossover from the two-phase model and single-phase model. Methanol concentration 1 M, cell temperature, 70 °C, methanol flow rate 6 ml min$^{-1}$, and air flow rate 1200 SCCM.

diffusion and electro-osmotic drag. Diffusion is caused by the methanol concentration gradient across the membrane. The electro-osmotic drag is caused by proton transfer through the membrane. When protons transfer from the anode to the cathode, water is dragged along. Since methanol is mixed with water and thus it is also dragged from the anode to the cathode. Therefore, drag coefficient for methanol is given by Eq. (44), from which it is clear that methanol flux due to electro-osmotic drag is proportional to its concentration at the anode/membrane interface. When the cell current density is about 0.073 A cm$^{-2}$, the pseudo-crossover current density reaches its maximum. This phenomenon is caused by the dual effect of current density on methanol crossover. The diffusion flux decreases with current density due to the consumption of methanol in the anode catalyst layer, causing a lower methanol gradient across the membrane. The flux due to electro-osmotic drag is proportional to both the concentration at the anode and the cell current density. As current density increases, the product of methanol concentration and $\lambda_w$ may reach a maximum. Fig. 5 shows an example of comparison between the results of methanol crossover pseudo-current densities from the single-phase model and the two-phase model. It is clear that the single-phase model significantly under-predicts the methanol crossover.

### 4.3. Anode liquid saturation

Fig. 6 shows a contour plot of anode liquid saturation at current density of 0.367 A cm$^{-2}$ and anode overpotential of 0.52 V.

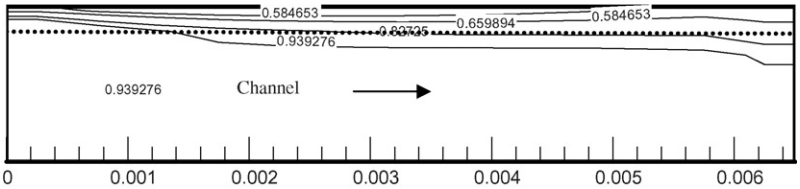


Fig. 6. Contour plot of anode liquid saturation. Cell current density, 0.367 A cm$^{-2}$ and anode overpotential 0.52 V, methanol concentration, 1 M, and cell temperature, 70 °C, methanol flow rate 6 ml min$^{-1}$, and air flow rate 1200 SCCM.

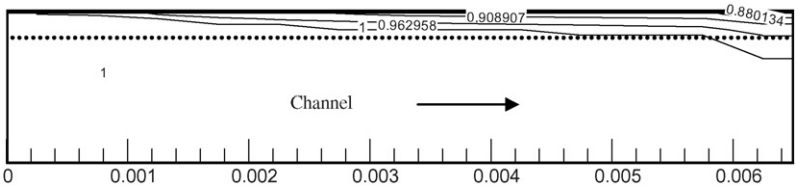


Fig. 7. Contour plot of anode liquid saturation. Cell current density, 0.192 A cm$^{-2}$ and anode overpotential 0.4 V, methanol concentration, 1 M, and cell temperature, 70 °C, methanol flow rate 6 ml min$^{-1}$, and air flow rate 1200 SCCM.

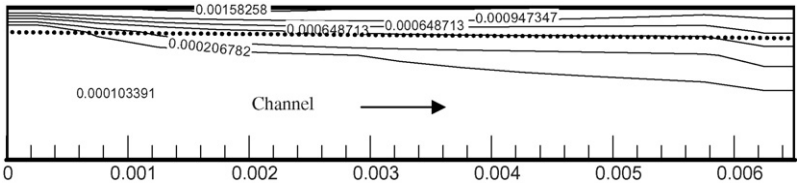


Fig. 8. The contour plot of total carbon dioxide mass fraction at current density 0.367 A cm$^{-2}$, anode overpotential 0.52 V, and anode GDL porosity of 0.6, methanol flow rate 6 ml min$^{-1}$, and air flow rate 1200 SCCM.

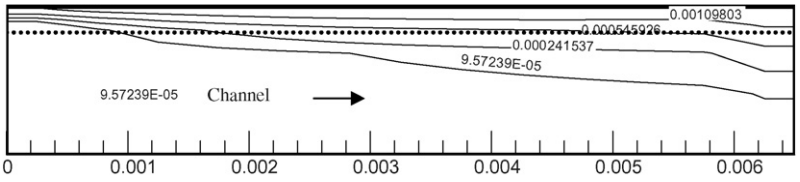


Fig. 9. The contour plot of total carbon dioxide mass fraction at current density 0.51 A cm$^{-2}$, anode overpotential 0.52 V, the anode GDL porosity of 0.7, methanol flow rate 6 ml min$^{-1}$, and air flow rate 1200 SCCM.

Since the gas saturation satisfies $s_l + s_g = 1$, it is clear that gas volume fraction increases along the channel due to the accumulation from upstream. The modeling result also showed that the gas volume fraction in the catalyst layer can be as high as more than 40%. With such a high gas volume, a significant fraction of the catalyst surface can be made inactive. Fig. 7 shows another contour plot of anode liquid saturation at current density of 0.192 A cm$^{-2}$ and anode overpotential 0.40 V. Comparing it with Fig. 6, it can be seen that higher liquid fraction or lower carbon dioxide gas fraction exists at lower current density.

### 4.4. Carbon dioxide mass fraction

Fig. 8 shows the distribution of carbon dioxide mass fraction along the channel direction. Note that the mass fraction includes the masses of both the dissolved and gaseous carbon dioxide. The carbon dioxide mass fraction at the inlet is zero, and along the channel as electrochemical reaction occurs and the methanol is consumed, the carbon dioxide mass fraction increases. The amount of carbon dioxide created is proportional to the current density. Firstly, carbon dioxide dissolves in water and when it reaches its solubility limit, carbon dioxide gas emerges. At the same flow rate, the higher the current density is, the higher is the carbon dioxide mass fraction.

Fig. 9 shows another result of distribution of carbon dioxide mass fraction. All the parameters are the same as those in Fig. 8 except the porosity of the diffusion layer, which is 0.7, greater than that in Fig. 8. Due to the higher porosity of the diffusion layer, the corresponding current density is higher. Comparing with Fig. 8, it can be seen that the case shown in Fig. 9 has lower carbon dioxide concentration in the catalyst layer even though it has a higher current density. This means that a higher porosity in the diffusion layer lead to more effective removal of carbon dioxide gas, thus reducing the blockage of the catalyst surface area, resulting in higher current density and better cell performance.

Fig. 10 shows the distribution of $CO_2$ mass fraction along $z$-direction and at the different locations along the flow direction. It can be seen that near the channel inlet, the $CO_2$ mass fraction

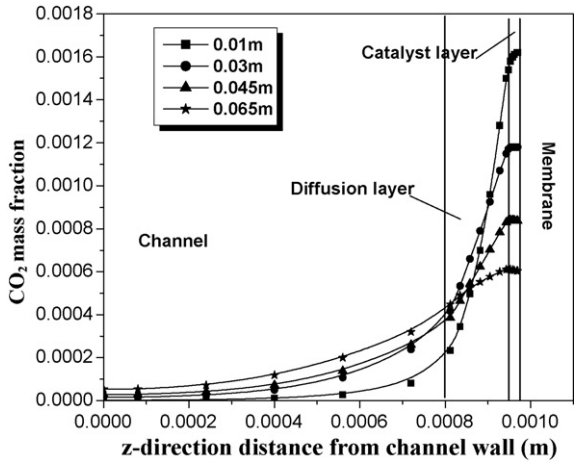


Fig. 10. Distribution of $CO_2$ mass fraction along $z$-direction at different locations along the flow direction. Methanol concentration 1 M, cell temperature, 70 °C, methanol flow rate 6 ml min$^{-1}$, and air flow rate 1200 SCCM.

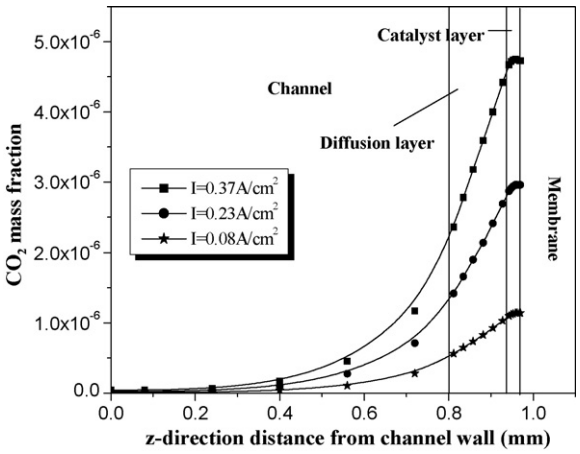


Fig. 11. Average $CO_2$ mass fraction profiles at different current densities. Methanol concentration 1 M, cell temperature, 70 °C., methanol flow rate 6 ml $min^{-1}$, and air flow rate 1200 SCCM.

is higher in the catalyst layer due to the higher current density. Since current density decrease along the channel direction the $CO_2$ mass fraction also decreases along the channel direction. But $CO_2$ mass fraction in the channel is lower near the inlet and increase along the flow direction. This is caused by the accumulation of the generated $CO_2$. Fig. 11 shows the average $CO_2$ mass fraction variation along the $z$-direction at different average cell current densities. The averaged values are taken over the entire channel, form the inlet to the outlet. It is clear that the higher the current density is the higher is the $CO_2$ mass fraction. Since $CO_2$ is generated in the catalyst layer and transfer out through the diffusion layer to the channel, the highest $CO_2$ mass fraction occurs in the catalyst layer. The dominant mass transfer mode in the diffusion layer is diffusion, so the profile of $CO_2$ mass fraction in the diffusion layer is almost linear even after taking the average value.

## 5. Concluding remarks

A three-dimensional, two-phase, multi-component model has been developed for a liquid-fed DMFC. The anode and cathode catalyst layer are considered as parts of the modeling domain instead of interfaces. The model incorporates the effects of the second phase on the reduction of active catalyst surface areas and the mixed potential effects due to methanol crossover. At the anode side the presence of gas phase reduces the active catalyst areas, while at the cathode side the presence of liquid water reduces the active catalyst areas. The modeling results of polarization curves show good agreement with the experimental data. Compared with the single-phase model, the two-phase model shows better agreement with the experimental data, especially at high current densities. Further comparisons show that the single-phase model under-predicts the anode overpotential as well as the rate of methanol crossover, and the amounts of under prediction increase with current density. The modeling results of $CO_2$ mass fraction showed that the porosity of the anode diffusion layer played a very important role in the DMFC performance. With a low porosity, the produced carbon dioxide cannot be removed effectively from the catalyst layer, thus reducing the active catalyst surface area as well as blocking methanol from reaching the reaction zone.

## References

[1] S.F. Baxter, V.S. Battaglia, R.E. White, J. Electrochem. Soc. 146 (2) (1999) 437–447.
[2] H. Dohle, H. Schmitz, T. Bewer, J. Mergel, D. Stolten, J. Power Sources 106 (2002) 313–322.
[3] P. Argyropoulos, K. Scott, W.M. Taama, Chem. Eng. J. 78 (2000) 29–41.
[4] K. Scott, P. Argyropoulos, K. Sundmacher, J. Electroanal. Chem. 477 (1999) 97–110.
[5] K. Sundmacher, K. Scott, Chem. Eng. Sci. 54 (1999) 2927–2936.
[6] J. Cruickshank, K. Scott, J. Power Sources 70 (1998) 40–47.
[7] A.K. Shukla, C.L. Jackson, K. Scott, G. Murgia, J. Power Sources 111 (2002) 43–51.
[8] A.A. Kulikovsky, J. Appl. Electrochem. 30 (2000) 1005–1014.
[9] Z.H. Wang, C.Y. Wang, J. Electrochem. Soc. 150 (4) (2003) A508–A519.
[10] E. Birgersson, J. Nordlund, H. Ekstrom, M. Vynnycky, G. Lindbergh, J. Electrochem. Soc. 150 (10) (2003) A1368–A1376.
[11] J. Divisek, J. Fuhrmann, K. Gartner, R. Jung, J. Electrochem. Soc. 150 (6) (2003) A811–A825.
[12] C.Y. Wang, Chem. Rev. 104 (2004) 4727–4766.
[13] H. Liu, T. Zhou, P. Cheng, J. Heat Transfer 127 (2005) 1363–1379.
[14] A.Z. Webber, J. Newman, Chem. Rev. 107 (2004) 4672–4726.
[15] Z.H. Wang, C.Y. Wang, K.S. Chen, J. Power Sources 94 (2000) 40–50.
[16] L. You, H. Liu, Int. J. Hydrogen Energy 26 (2001) 991–999.
[17] T. Berning, N. Djilali, J. Electrochem. Soc. 150 (12) (2003) A1598–A1607.
[18] W. He, J.S. Yi, T. Van Nguyen, AIChe J. 45 (October (10)) (2000).
[19] C.Y. Wang, P. Cheng, Int. J. Heat Mass Transfer 39 (1996) 3607–3618.
[20] P. Cheng, C.Y. Wang, Int. J. Heat Mass Transfer 39 (1996) 3619–3632.
[21] P. Argyropoulos, K. Scott, W.M. Taama, Electrochim. Acta 44 (1999) 3575–3584.
[22] D. Natarajan, T. Van Nguyen, J. Electrochem. Soc. 148 (12) (2001) A1324–A1335.
[23] T.E. Springer, T.A. Zawodzinski, S. Gottesfeld, J. Electrochem. Soc. 138 (8) (1991) 2334–2342.
[24] U. Sukkee, C.-Y. Wang, K.S. Chen, J. Electrochem. Soc. 147 (12) (2000) 4485–4493.
[25] X. Ren, T.E. Springer, T.A. Zawodzingski, S. Gottesfeld, J. Electrochem. Soc. 147 (2000) 466.
[26] J. Ge, H. Liu, J. Power Sources 142 (2005) 56–69.